Atomic layer deposition of tin oxide films using tetrakis(dimethylamino) tin

Jeffrey W. Elam,[a] David A. Baker, and Alexander J. Hryn
Argonne National Laboratory, Argonne, Illinois 60439

Alex B. F. Martinson
Argonne National Laboratory, Argonne, Illinois 60439
and Department of Chemistry, Northwestern University, Evanston, Illinois 60208

Michael J. Pellin
Argonne National Laboratory, Argonne, Illinois 60439

Joseph T. Hupp
Department of Chemistry, Northwestern University, Evanston, Illinois 60208

(Received 17 September 2007; accepted 19 December 2007; published 29 January 2008)

The authors present a new method for preparing thin films of SnO_2 by atomic layer deposition (ALD) using alternating exposures to tetrakis(dimethylamino) tin and hydrogen peroxide. This method avoids problems of corrosion and agglomeration associated with the halogenated compound, $SnCl_4$. Tin oxide films were successfully deposited on a variety of substrates using deposition temperatures of 50–300 °C at an average growth rate of 1.2 Å/cycle. They use *in situ* quartz crystal microbalance and quadrupole mass spectrometry measurements to explore the mechanism for SnO_2 ALD. Scanning electron microscopy of SnO_2 films deposited on Si(100) show that the SnO_2 films are smooth, conformal, and nearly featureless, while atomic force microscopy yields a surface roughness of only 0.84 nm for a film with a thickness of 92 nm. X-ray diffraction reveals that the SnO_2 films are amorphous. Films deposited on glass yielded a resistivity of ~0.3 Ω cm and an optical transmission of 94% for a film thickness of 140 nm. X-ray photoelectron spectroscopy measurements were consistent with residual dimethylamine ligands remaining in the film at deposition temperatures below 150 °C. This method allows, for the first time, low temperature (50 °C) growth of SnO_2 films by ALD. Additionally, they show that this process is suitable for conformally coating high aspect ratio anodic alumina membranes. © *2008 American Vacuum Society.* [DOI: 10.1116/1.2835087]

I. INTRODUCTION

Tin oxide is a transparent, conducting oxide with applications in numerous technologies including photovoltaics,[1] gas sensing,[2–6] catalysis,[7] optoelectronics,[8,9] and coatings for architectural glass.[10] Tin oxide is often doped with fluorine[11] or antimony[12] to improve the electrical conductivity. In addition, tin oxide is commonly used to dope indium oxide films to make indium tin oxide,[8,13,14] which is of one the most industrially important transparent conducting oxides.

For many of these applications, it is advantageous to apply the tin oxide as a thin film and this can be accomplished in different ways. For instance, SnO_2 thin films have been deposited previously using dc magnetron sputtering,[5] chemical vapor deposition,[15] spray pyrolysis,[11] and atomic layer deposition (ALD).[16–18] ALD is a thin film growth method utilizing alternating, self-limiting chemical reactions between gaseous precursors and a solid surface to deposit materials in an atomic layer-by-layer fashion.[19] This method can produce films with exquisite control over thickness and composition, and allows precise coatings to be applied on all exposed surfaces of nanoporous substrates such as powders or mesoporous membranes.[20,21]

SnO_2 films have been fabricated previously by ALD using the halogenated precursors $SnCl_4$ (Refs. 16 and 17) and SnI_4.[18] The disadvantages of these methods include relatively low growth rates, the need for high deposition temperatures, and the inconvenience of using halogenated precursors. Both the $SnCl_4$ and the HCl by-products are corrosive and can damage the deposition equipment. In some cases, halogenated precursors can even etch the deposited film.[22] Furthermore, halogenated precursors can form agglomerates when very large exposures are used to infiltrate porous substrates such as powders or nanoporous membranes leading to nonuniform coatings.[23] SnO_2 films have also been deposited previously using plasma assisted ALD.[24–26] However, this method suffers from the disadvantage that the plasma species are highly reactive and do not allow conformal coatings at very high aspect ratios.

One of our current research efforts is aimed at creating nanostructured, dye-sensitized solar cells by utilizing ALD methods to functionalize nanoporous solids.[27] This application demands ALD processes that provide high conformality at extremely large aspect ratios. To this end, we recently developed an ALD technique for depositing transparent, conducting In_2O_3 films using cyclopentadienyl indium and ozone.[28] In the current study, we continue this research endeavor and describe an improved ALD method for depositing SnO_2 using stable, nonhalogenated precursors. For the tin

[a]Electronic mail: jelam@anl.gov

precursor, we selected tetrakis(dimethylamino) tin (TDMASn), because similar precursors including TDMATi,[29] tetrakis(diethylamino) aluminum,[30] $W_2(NMe_2)_6$,[31] TDMAZr,[32] and TDMAHf (Ref. 32) have been used successfully for ALD of the corresponding metal oxides. As oxygen sources, we tested H_2O, H_2O_2, and O_3 and discovered that H_2O_2 yields the highest SnO_2 growth rates. *In situ* quartz crystal microbalance (QCM) and quadrupole mass spectrometry (QMS) measurements were used to explore the ALD growth mechanism. SnO_2 thin films were deposited on Si(100) and glass substrates and characterized using four point probe measurements, spectroscopic ellipsometry, x-ray diffraction (XRD), x-ray photoelectron spectroscopy (XPS), atomic force microscopy (AFM), and scanning electron microscopy (SEM).

II. EXPERIMENT

The ALD experiments used a viscous flow reactor[33] constructed from a circular, stainless steel flow tube with an inside diameter of 5 cm to hold the substrates for film growth as well as the QCM. Ultrahigh purity (99.999%) nitrogen carrier gas continuously passes through the flow tube at a mass flow rate of 360 sccm (standard cubic centimeters per minute) and a pressure of 1 Torr. A constant reactor temperature is maintained by four separate temperature controllers connected to resistive heating elements attached to the outside of the reactor. These four heating zones establish a uniform temperature profile along the length of the flow tube to minimize artifacts caused by temperature transients during the QCM measurements.[34]

SnO_2 ALD was performed using alternating exposures to tetrakis(dimethylamino) tin (TDMASn, Gelest, >95% purity) and hydrogen peroxide (H_2O_2, Aldrich, 50 wt % in water). TDMASn is a liquid at room temperature, and at 40 °C the vapor pressure is ~0.04 Torr. The TDMASn is held in a stainless steel bubbler maintained at 40 °C, and the tubing connecting the bubbler to the ALD reactor is maintained at 150 °C to prevent condensation of the TDMASn on the reactor walls. Ultrahigh purity nitrogen at a mass flow rate of 60 sccm was sent through the bubbler during the TDMASn exposures, and was diverted to bypass the bubbler following the TDMASn exposures. Additional oxygen sources evaluated for SnO_2 ALD included deionized water (18 MΩ cm) and ozone. The ozone was produced using a commercial ozone generator (Ozone Engineering L11) using a feed of ultrahigh purity oxygen at a flow rate of 400 sccm to produce ~10% ozone in oxygen.

The ALD timing sequences can be expressed as $t1:t2:t3:t4$ where $t1$ is the exposure time for the first precursor, $t2$ is the purge time following the first exposure, $t3$ is the exposure time for the second precursor, and $t4$ is the purge time following the exposure to the second precursor where the units are in seconds. The typical timing sequence for SnO_2 ALD was 1:5:1:5.

To enable *in situ* measurements during the SnO_2 ALD, a QCM was installed in the ALD reactor in place of the substrates. These studies utilized a Maxtek BSH-150 bakeable sensor, AT-cut quartz sensor crystals with a polished front surface (Colorado Crystal Corporation, part No. CCAT1BK-1007-000), and a Maxtek TM400 film thickness monitor interfaced to a personal computer. The ALD reactor was also equipped with a quadrupole mass spectrometer (Stanford Research Systems RGA300) located downstream of the QCM in a differentially pumped chamber separated from the reactor tube by a 35 μm orifice and evacuated using a 50 l/s turbomolecular pump.

The ALD SnO_2 films were deposited on 1×2 cm^2 Si(100) and glass substrates. Prior to loading, the substrates were cleaned in an ultrasonicator using acetone and then isopropanol and blown dry using nitrogen. After loading, the substrates were allowed to outgas in the ALD reactor for 10 min at the deposition temperature (typically 175 °C) in 1 Torr of flowing ultrahigh purity nitrogen. Next, the substrates were cleaned *in situ* using a 60 s exposure to 10% ozone in oxygen at a pressure of 2 Torr and a mass flow rate of 400 sccm. Before the ALD SnO_2, we first deposited ~1 nm ALD Al_2O_3 using ten cycles of trimethyl aluminum (Aldrich) and H_2O_2. This ALD Al_2O_3 layer was used to promote prompt nucleation of the ALD SnO_2 as a result of the chemically uniform surface and high density of surface hydroxyl groups. When we omitted this initial Al_2O_3 coating step, we measured greater thickness variations in the thinner SnO_2 films.

SEM images were acquired using a Hitachi S4700 with a field emission gun electron beam source, secondary electron and backscattered electron detectors, and an energy dispersive analysis of x-rays detector for elemental analysis. AFM measurements were performed on a Digital Instruments Dimension 3000 with a NanoScope IIIa controller operated in tapping mode. XRD measurements were taken on a Rigaku Miniflex Plus diffractometer. Ellipsometric measurements were performed using a J. A. Woolam Co. M2000V variable angle spectroscopic ellipsometer (VASE) to determine the thickness and refractive index of the SnO_2 films deposited on Si(100) substrates. Optical absorption spectra were acquired from ALD SnO_2 films deposited on glass using the M2000V operated in transmission mode. Anodic aluminum oxide membranes (AAO, Whatman Anodisc 13) with pore diameters of 200 nm and a membrane thickness of 70 μm were also coated by SnO_2 to evaluate the ability of the TDMASn precursor to infiltrate porous materials. Prior to cross-sectional SEM analysis of cleaved specimens, the coated AAO membranes were annealed in air at 400 °C for 30 min to crystallize the SnO_2 thereby enhancing the contrast between the SnO_2 film and the AAO substrate.

XPS of the tin oxide films was performed in a separate XPS apparatus maintained at $\sim 1 \times 10^{-10}$ Torr using Mg $K\alpha$ (1253.6 eV) radiation and a hemispherical electron energy analyzer. Photoelectrons from the sample were collected from an elliptical area with 4×3 mm^2 dimensions. Survey spectra were recorded with energy steps of 1 eV and high-resolution scans of the Sn3$d_{5/2}$, O1s, C1s, and N1s peaks used energy steps of 0.1 eV. The molar concentrations of tin, oxygen, carbon, and nitrogen were obtained by subtracting a

Shirley background from the high resolution scans and comparing the Sn3$d_{5/2}$, O1s, C1s, and N1s peak areas using a relative sensitivity factor based on Scofield calculations.

III. RESULTS AND DISCUSSION

A. Mechanism for SnO_2 ALD

In this section we will evaluate the mechanism for SnO_2 ALD films based on *in situ* QCM and QMS measurements. In the next section, we will describe the growth of the SnO_2 films and demonstrate saturation of the individual ALD reactions as well as linearity of the film thickness as a function of the number of ALD cycles. Finally, in the last section we will examine the properties of the SnO_2 films. We will begin our exploration of the mechanism for SnO_2 ALD using QCM measurements. Figure 1(a) shows the thickness versus time measured by *in situ* QCM for SnO_2 ALD with the timing sequence 1:5:1:5 at a temperature of 150 °C. The QCM data demonstrate linear growth and yield a growth rate of 0.96 Å/cycle assuming a density for the deposited film of 6.95 g/cm^3. Figure 1(b) presents an expanded view of the QCM data illustrating the structure of the QCM steps. This structure is dictated by the ALD SnO_2 growth mechanism, and one such mechanism is

$$OH_x^* + Sn(DMA)_4 \rightarrow (O)_xSn(DMA)_{4-x}^* + xHDMA, \quad (1)$$

$$(O)_xSn(DMA)_{4-x}^* + 2H_2O_2 \rightarrow O_2Sn(OH)_x^* + 4 - xHDMA + O_2. \quad (2)$$

In these equations, the asterisks represent the surface species, DMA is the dimethylamino ligand, HDMA is dimethylamine, and x is the number of DMA ligands released during the TDMASn exposures. Using the relationship $R=\Delta m/\Delta m_1$, where Δm is the mass change from one complete cycle and Δm_1 is the mass change after reaction (1), we calculate from Eqs. (1) and (2) and the atomic masses that $\Delta m=(SnO_2)=151$ and $\Delta m_1=(Sn)+(4-x)(DMA)-x(H)=295-45x$ so that $R=151/(295-45x)$. From Fig. 1(b), $R=0.99$ so that $x=3.2$ which implies that, on average, 20% of the DMA ligands remain on the surface after reaction (1).

Steric hindrance is known to limit ALD growth rates.[35] For instance, a smaller value of x in Eq. (1) would imply that more ligands are left on the SnO_2 surface following the TDMASn exposures. The increased steric hindrance imposed by these extra DMA ligands will inhibit TDMASn adsorption, thereby lowering the SnO_2 growth rate. To test this hypothesis, QCM data was recorded during alternating TDMASn/H_2O exposures under conditions similar to those used for Fig. 1. Analysis of this data yielded $R=0.83$ so that $x=2.5$ implying that, on average, 37% of the DMA ligands remain on the surface. As shown in Fig. 4, H_2O yields a lower growth rate when compared to H_2O_2, suggesting that steric hindrance may indeed control the SnO_2 growth rate.

Next, we turn to the *in situ* QMS measurements. A variety of masses were observed during the SnO_2 ALD including $m/e=44$, 45, and 18 at relative intensities consistent with the cracking pattern of dimethylamine.[36] Figure 2 shows QMS measurements performed during the SnO_2 ALD monitoring $m/e=44$. These experiments used the timing sequence 0.7:20:1:20 at a temperature of 150 °C. Dimethylamine is observed during both the TDMASn and the H_2O_2 exposures in agreement with the mechanism given in Eqs. (1) and (2). The relative amount of dimethylamine released during the TDMASn and H_2O_2 exposures can be obtained by integrating the $m=44$ signals observed during the individual half-reactions, and this ratio can be used to calculate the unknown quantity x in Eqs. (1) and (2). After subtracting the background signals observed when the TDMASn and H_2O_2 were

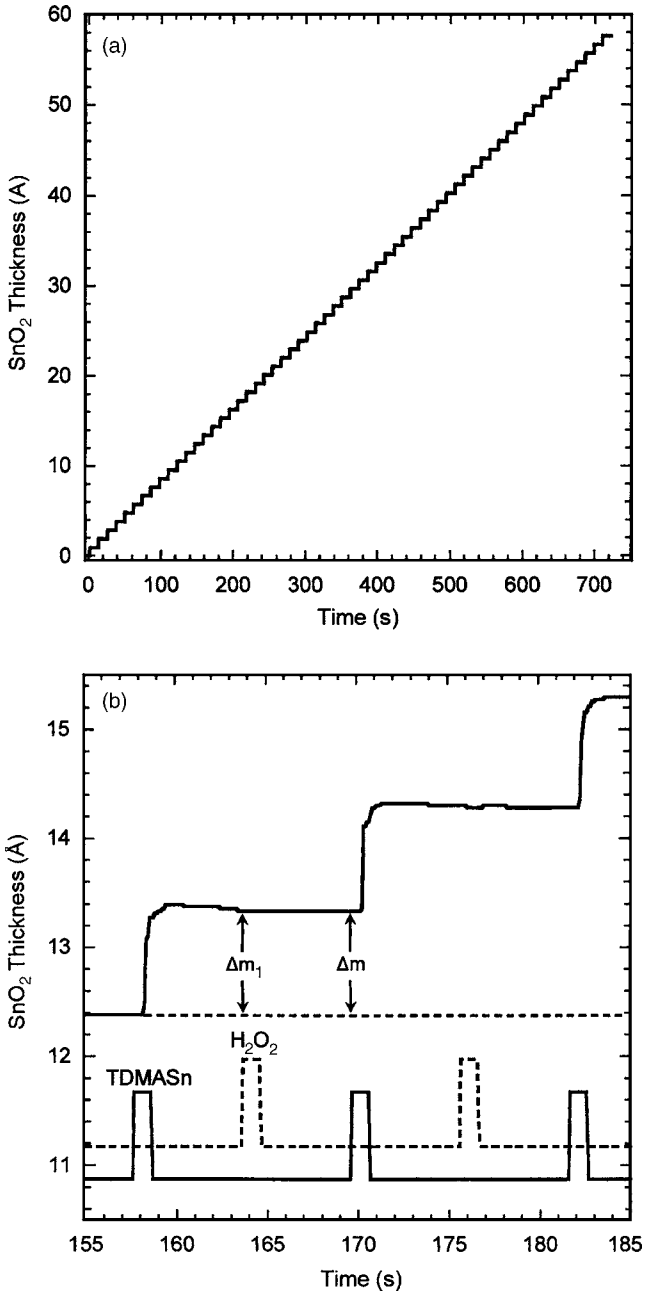

FIG. 1. (a) SnO_2 film thickness vs time as determined by *in situ* QCM using the timing sequence 1:5:1:5 at 150 °C illustrating linear growth. (b) Expanded view of QCM data revealing mass changes observed during individual TDMASn and H_2O_2 exposures.

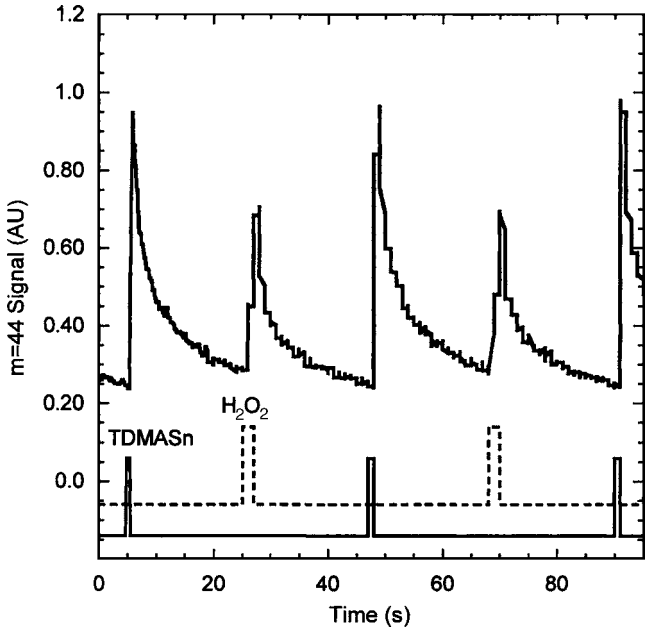

FIG. 2. $m=44$ signal from dimethylamine vs time as determined by *in situ* QMS during SnO_2 ALD using the timing sequence 0.7:20:1:20 at 150 °C. After background subtraction, the relative amount of dimethylamine product released during TDMASn and H_2O_2 exposures can be determined.

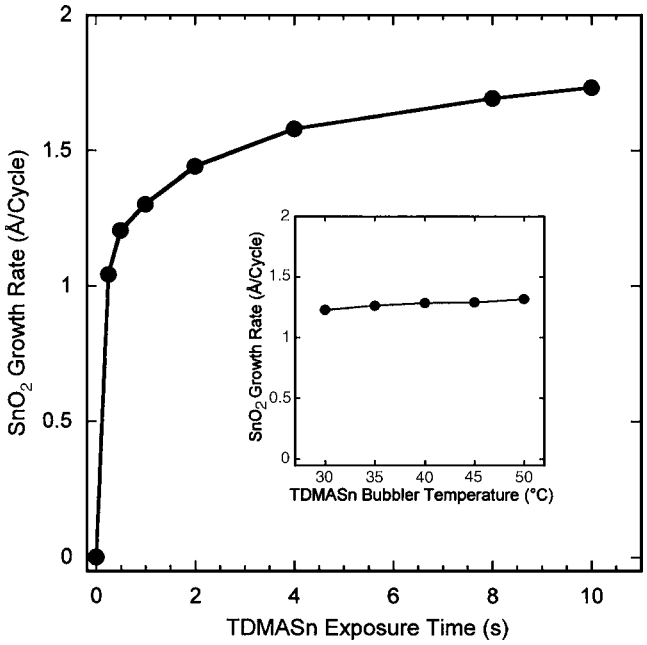

FIG. 3. SnO_2 growth rate vs TDMASn exposure time measured using ellipsometry for films deposited on Si(100) with the timing sequence $x:5:1:5$ at 175 °C. Inset shows the effect of varying the TDMASn bubbler temperature on the SnO_2 growth rate using the timing sequence 1:5:1:5.

pulsed independent of the other reactant, the $m=44$ mass ratio is $x/(4-x)=3.2$, so that $x=3.0$. In other words, three of the four DMA ligands are lost during the reaction of TDMASn with the hydroxylated surface. This value agrees very well with the value $x=3.2$ obtained from the QCM measurements, and supports the conclusion that only ~20%–23% of the DMA ligands remain following the TDMASn exposures.

The relatively long tails on the QMS signals observed for $m=44$ most likely result from strong physisorption and subsequent slow desorption of the DMA molecules from the surfaces of the QMS chamber. Although the inlet surfaces of the QMS chamber are heated to 150 °C, the surfaces close to the QMS electron multiplier are not heated, and, consequently, these surfaces will adsorb the DMA more strongly and increase the DMA residence time.

In addition to the DMA mass signals, we also observed $m=32$ signals from O_2 produced during the SnO_2 ALD, as predicted by Eq. (2). The $m=32$ signal attributed to O_2 from the reaction of H_2O_2 with the DMA-saturated SnO_2 surface appeared as brief, high intensity spikes and were easily differentiated from the broad, lower intensity $m=32$ signals arising from the thermal decomposition of H_2O_2 on the reactor walls. As expected, we did not observe the O_2 reaction product during SnO_2 ALD using H_2O. These findings support the mechanism given in Eqs. (1) and (2).

B. Growth of SnO_2 films

Figure 3 shows the effect of varying the TDMASn exposure time on the growth rate of SnO_2. These measurements were performed on SnO_2 films deposited on Si(100) substrates using 100 TDMASn/H_2O_2 cycles at 175 °C with the timing sequence $x:5:1:5$ after first depositing ~1 nm ALD Al_2O_3. The film thicknesses in Figs. 3–6 were determined using VASE measurements. For the longer TDMASn exposures exceeding 2 s, the purge times following the TDMASn exposures were also increased to prevent chemical vapor deposition. Figure 3 demonstrates that the SnO_2 growth rate increases sharply with TDMASn exposure times up to ~1 s,

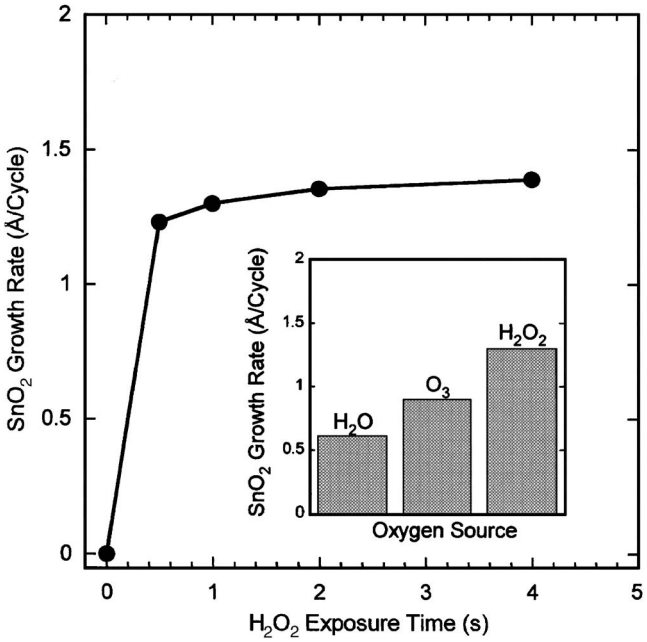

FIG. 4. SnO_2 growth rate vs H_2O_2 exposure time measured using ellipsometry for films deposited on Si(100) with the timing sequence $1:5:x:5$ at a temperature of 175 °C. Inset shows the effect of varying the oxygen source (H_2O, O_3, and H_2O_2) on the SnO_2 growth rate.

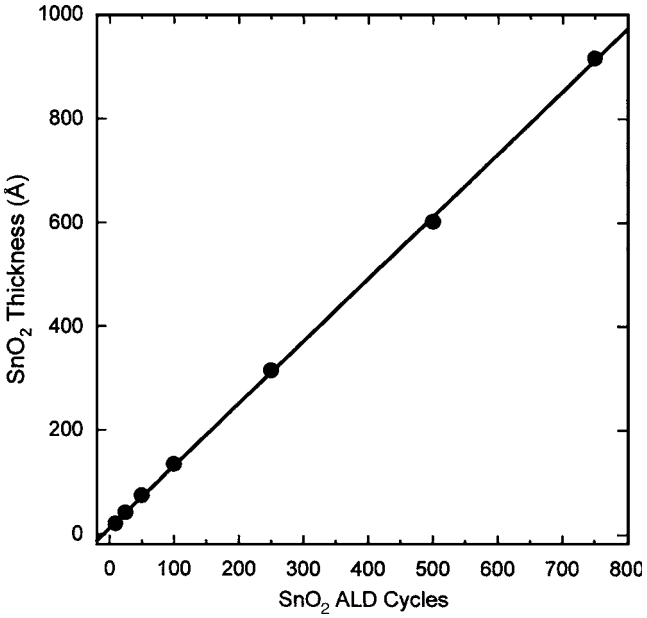

FIG. 5. SnO_2 film thickness vs number of cycles measured using ellipsometry for films deposited on Si(100) at 175 °C using the timing sequence 1:5:1:5 yielding growth rate of 1.2 Å/cycle.

and then increases gradually for larger exposure times. It is not clear from this figure whether the TDMASn exposures are saturating. To further explore the effect of the TDMASn exposure, we kept the ALD timing sequence at 1:5:1:5 and varied the temperature of the TDMASn bubbler from 30 to 50 °C to adjust the TDMASn vapor pressure. As shown by the inset in Fig. 3, increasing the TDMASn bubbler temperature above 30 °C barely affects the SnO_2 growth rate and argues for self-limiting growth.

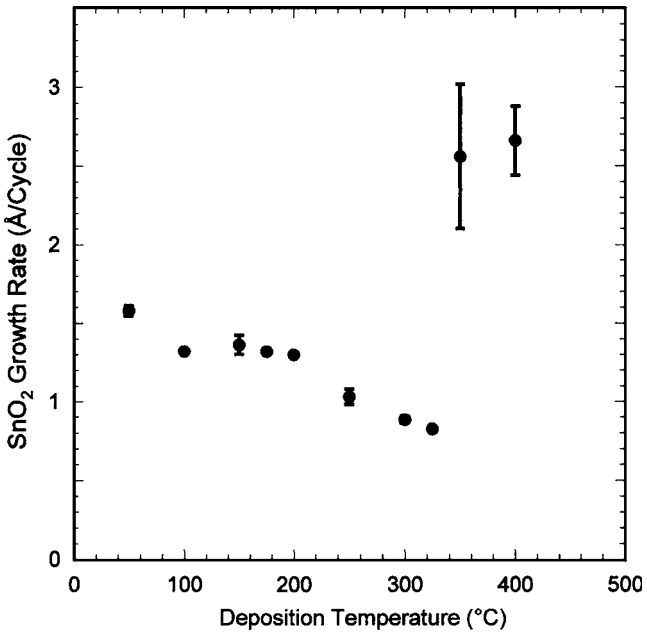

FIG. 6. SnO_2 growth rate versus deposition temperature in the range of 50–400 °C measured by ellipsometry for films deposited on Si(100) using the timing sequence 1:5:1:5. The error bars represent the standard deviation values for thickness measurements obtained from different samples.

The gradual saturation observed with increasing TDMASn exposure times is similar to previous measurements of TiO_2 and HfO_2 ALD using TDMATi (Ref. 37) and tetrakis(ethylmethyl)amino hafnium (TEMAHf),[38] respectively. In the case of TiO_2, the non-self-limiting behavior was attributed to thermal decomposition of the TDMATi,[37] while the gradual saturation using TEMAHf was believed to result from slow adsorption kinetics.[38] It is unlikely that the gradual increase in Fig. 3 arises from thermal decomposition of the TDMASn precursor because these films were deposited at 175 °C, and we clearly see the onset of TDMASn thermal decomposition at a much higher temperature of 350 °C (Fig. 6). However, the slow saturation of the TDMASn reaction may result from slow desorption of the DMA product. DMA is likely to bind strongly to the hydroxylated SnO_2 surface. For instance, the desorption of DMA from TiN following TDMATi exposures occurs very slowly and requires ~100 s at 128 °C.[39] Only after DMA desorbs from the SnO_2 surface can additional TDMASn molecules react to form a saturated monolayer. This hypothesis could be tested by checking for an increase in SnO_2 growth rate with increasing purge times. Although we found no change in SnO_2 growth rate when the TDMASn and H_2O_2 purge times were varied in the range of 2–10 s, perhaps TDMASn purge times >10 s are required to observe the effect of complete DMA desorption.

Figure 4 shows the variation in SnO_2 growth rate with increasing H_2O_2 exposure times. These growth rates were determined from SnO_2 films deposited on Si(100) substrates using 100 TDMASn/H_2O_2 cycles at 175 °C with the timing sequence $1:5:x:5$ after first depositing ~1 nm ALD Al_2O_3. Figure 4 demonstrates that the SnO_2 growth rate is saturated at 1.3 Å/cycle for H_2O_2 exposure times of ~1 s.

The inset in Fig. 4 shows the effect of varying the oxygen source on the ALD SnO_2 growth rate at a deposition temperature of 175 °C. H_2O_2 yields the highest growth rate of 1.3 Å/cycle while O_3 and H_2O give 0.89 and 0.61 Å/cycle, respectively. Previously, H_2O_2 has been shown to enhance SnO_2 growth compared with H_2O for ALD using $SnCl_4$ (Ref. 17) and also for films deposited by spray pyrolysis.[11] Additionally, such an effect has been observed for In_2O_3 ALD using $InCl_3$.[40] It is believed that H_2O_2 produces a higher concentration of surface hydroxyl groups than H_2O and this causes a higher growth rate.

Figure 5 shows the effect of varying the number of TDMASn/H_2O_2 cycles between 10 and 750 cycles. These films were deposited on Si(100) substrates at 175 °C using the timing sequence 1:5:1:5 after first depositing ~1 nm ALD Al_2O_3. This figure yields an average growth rate of 1.2 Å/cycle. However, the growth rate determined from discrete points on this graph decreases from 2.03 Å/cycle at 10 cycles to 1.22 Å/cycle at 750 cycles. This decrease suggests an enhanced reactivity of the TDMASn precursor on the initial Al_2O_3 surface compared with the final SnO_2 sur-

face. The growth rate of 1.2 Å/cycle measured by ellipsometry for SnO_2 films deposited at 150 °C using the 1:5:1:5 timing is larger than the corresponding growth rate of 0.96 Å/cycle measured by QCM. This discrepancy may imply that the SnO_2 films have a lower density than the value of 6.95 g/cm^3 used to convert the QCM data. Alternatively, the QCM surface may experience slightly lower TDMASn exposures than the Si substrates. The SnO_2 growth rate of 1.2 Å/cycle is significantly higher than the growth rate of 0.7 Å/cycle measured previously using $SnCl_4$.[17]

The variation in SnO_2 growth rate with deposition temperature between 50 and 350 °C is presented in Fig. 6. These films were prepared using 100 TDMASn/H_2O_2 cycles on Si(100) substrates using the timing sequence 1:5:1:5 after first depositing ~1 nm ALD Al_2O_3. The SnO_2 growth rate decreases steadily from 1.58 Å/cycle at 50 °C to 0.83 Å/cycle at 325 °C. This gradual decrease is consistent with a decrease in the number of surface hydroxyl groups as has been observed previously for ALD Al_2O_3.[41] The SnO_2 growth rate increases abruptly to 2.56 Å/cycle at 350 °C and the films become less uniform in thickness as indicated by the large error bars measured at 350 and 400 °C in Fig. 6. These findings indicate the onset of thermal decomposition of the TDMASn precursor at 350 °C leading to non-self-limited growth.

C. Properties of SnO_2 films

The refractive indices at 633 nm determined from VASE measurements of the ALD SnO_2 films deposited using 100 cycles versus the deposition temperature are shown in Fig. 7(a). Above 200 °C, the refractive index for the SnO_2 films was relatively constant at $n=1.83-1.91$. Below 200 °C, the refractive index decreased steadily with deposition temperature to $n=1.62$ at 50 °C. Figure 7(b) shows the C and N concentrations in the SnO_2 films versus deposition temperature determined using XPS measurements. Above 200 °C, the C content remains nearly constant at 5%–6% and the N content is undetectable. Below 200 °C, the C and N contents increase with decreasing deposition temperature reaching 10% and 2%, respectively, at 50 °C. We also evaluated the resistivity of the ALD SnO_2 films versus deposition temperature using four point probe measurements and found that the resistivity decreased from $\rho=2.8\times10^{-1}$ Ω cm at 150 °C to $\rho=1.9\times10^{-3}$ Ω cm at 200 °C. These resistivity values are comparable to those measured previously for SnO_2 films prepared using $SnCl_4$.[16]

The refractive index for the films deposited above 200 °C are consistent with the accepted value for bulk SnO_2 which is $n=1.9$. In addition, XPS shows no N in these films, and the constant value of 5%–6% carbon above 200 °C probably results from surface contamination after air transfer between the ALD reactor and the XPS system.[24] These results indicate that the films are relatively pure SnO_2 when deposited above 200 °C. The decrease in refractive index at lower temperatures suggests a lower density for the SnO_2 films and may result from the incorporation of impurities in the films such as unreacted DMA or OH ligands. The incorporation of impurities also explains the increase in resistivity for the lower deposition temperatures. If we assume that surface contamination contributes ~5% to the C XPS signals, then the C:N ratio in the films at the lower temperatures is ~2:1 as would be expected from dimethylamine. It is plausible that the surface reactions do not proceed to completion below 200 °C. Longer H_2O_2 exposures, or possibly employing O_3 or oxygen radicals in place of the H_2O_2, may yield higher purity SnO_2 films at lower temperatures.

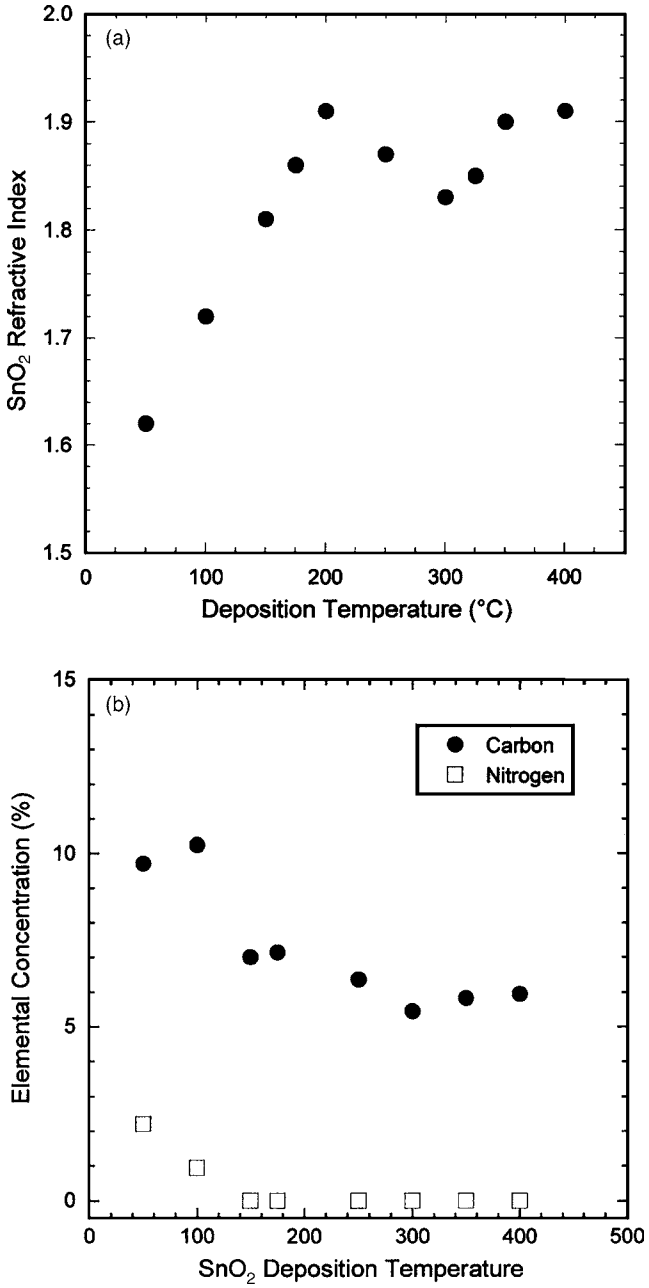

FIG. 7. (a) Refractive index of SnO_2 films measured using ellipsometry vs deposition temperature. (b) Nitrogen and carbon contents of SnO_2 films vs deposition temperature determined by XPS measurements.

We measured refractive indices of $n=1.83-1.91$ for films deposited above 200 °C, and XRD analysis indicated amorphous films. In contrast, ALD SnO_2 films deposited using

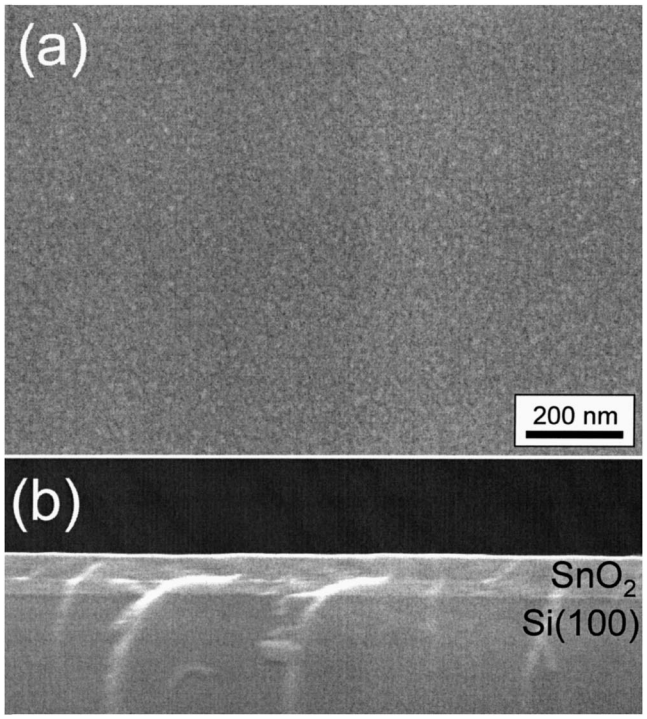

FIG. 8. Plan-view (a) and cross-sectional view (b) SEM images of SnO_2 film with a thickness of 916 Å deposited on Si(100) at a temperature of 150 °C.

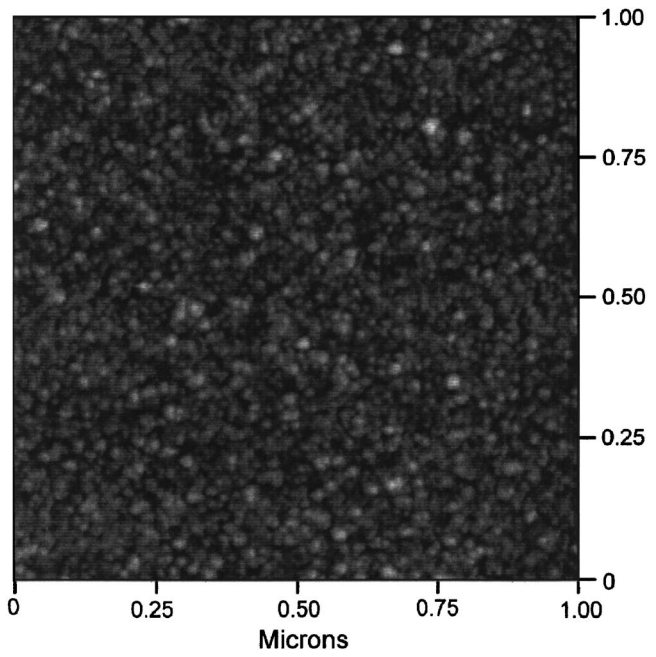

FIG. 9. AFM image of SnO_2 film with a thickness of 916 Å deposited on Si(100) at a temperature of 150 °C. The light-to-dark range of this image represents a height difference of 7.0 nm, and the film has a rms roughness of 0.85 nm.

$SnCl_4$ at 400–600 °C yielded a higher refractive index of $n=2.0$ and were polycrystalline.[12] Evidently, the amorphous SnO_2 films deposited using TDMASn are less dense than the polycrystalline films prepared using $SnCl_4$.

Figure 8(a) shows a plan-view SEM image of a SnO_2 film with a thickness of 916 Å deposited on Si(100) at 150 °C. The SEM image shows a smooth, featureless surface in agreement with the amorphous structure observed by XRD. The cross-sectional SEM image of this film [Fig. 8(b)] shows a conformal, flat film with no evidence of granularity as would be seen for a crystalline film. The film thickness determined from this SEM image is 93 nm, in excellent agreement with the ellipsometric thickness measurement of 91.6 nm. This close similarity lends confidence to the refractive index values derived from the ellipsometer.

Tin oxide can assume a range of stoichiometries including SnO, Sn_3O_4, and SnO_2.[42] For instance, ALD performed at 325 °C using $SnCl_4/H_2O_2$ produces substoichiometric SnO_x films with $x=1.1-1.5$,[17] while ALD performed at 500 °C using $SnCl_4/H_2O$ produces stoichiometric SnO_2 films.[16] The XPS measurements performed in this study yielded SnO_x with $x=0.95-1.4$, suggesting that the films are mostly SnO. However, because XPS only probes several nanometers of the film, this measurement probably reflects an oxygen deficient SnO surface layer.[43] Although the stoichiometry of the bulk of the ALD SnO_2 films was not determined, all of the bulk measurements indicate that it is oxygen deficient SnO_2. The refractive index of the films deposited above 200 °C ($n=1.83-1.91$) is in the accepted range for SnO_2 (1.85–2.1), but substantially lower than the refractive index of SnO ($n=2.4$). The conductivity of the films indicates that the films contain oxygen vacancies. Finally, thick films deposited on glass were highly transparent and did not have the characteristic brown color associated with SnO.[44]

An AFM image of an ALD SnO_2 film with a thickness of 916 Å deposited on Si(100) at a temperature of 150 °C is shown in Fig. 9. This z scale on this image has a light-to-

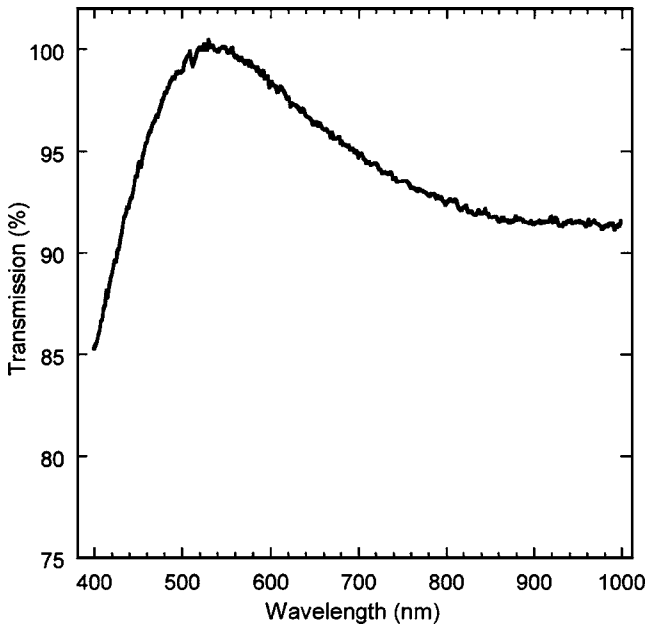

FIG. 10. Optical transmission vs wavelength measured from a SnO_2 film with a thickness of 140 nm deposited on glass at 150 °C. This spectrum is referenced to a bare glass substrate, and the average transmission over the wavelength range of 400–1000 nm is 94%.

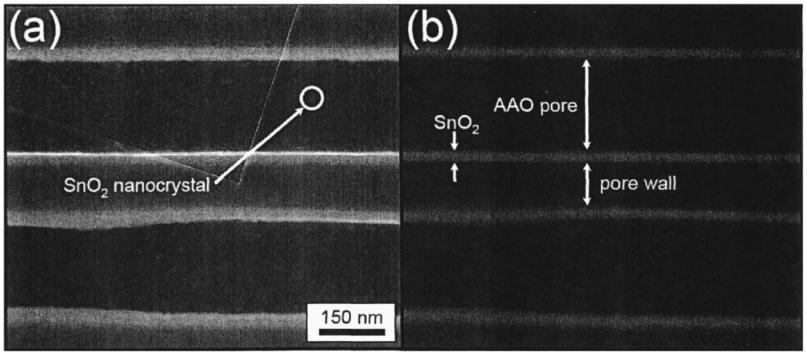

FIG. 11. SEM images acquired from middle of cleaved cross section of AAO membrane coated with 38 nm SnO_2. Images are recorded using secondary electron detector (a) and backscattered electron detector (b). Sample was annealed at 400 °C prior to analysis to induce crystallization and enhance contrast.

dark range of 7.0 nm, and the rms roughness is 0.85 nm. This rms roughness is significantly lower than the values of 4–12 nm measured previously for SnO_2 films prepared using $SnCl_4$,[45] but is typical for an amorphous metal oxide film deposited by ALD. A SnO_2 film with a thickness of 140 nm was deposited on a glass substrate at 150 °C. The optical transmission spectrum for this film is shown in Fig. 10. This spectrum has been referenced to an uncoated glass substrate, and yields an average transmission in the range of 400–1000 nm of $T=94\%$. This value is comparable to the transmission of SnO_2 films prepared using $SnCl_4$.[16]

To test ability of this new ALD SnO_2 process to generate conformal coatings at high aspect ratio, we coated an AAO membrane with a pore diameter of $d=200$ nm and a thickness of $L=60$ μm yielding an aspect ratio of $L/d=300$. After coating with a SnO_2 film of a thickness of 38 nm, the AAO membrane was annealed in air at 400 °C for 4 h to induce crystallization and enhance the SEM contrast. A SEM image recorded using secondary electron detection taken from the middle of a cleaved cross section of the coated AAO membrane is shown in Fig. 11(a). SnO_2 crystals are clearly visible on the inner surfaces of the two adjacent AAO pores, and the ALD SnO_2 film with a thickness of ~40 nm is also evident lining the inner walls of the two pores. The conformal SnO_2 films are more obvious in the backscattered electron image [Fig. 11(b)] recorded from the same region of the AAO membrane. The backscattered electron image provides high contrast because the SnO_2 (average atomic number $z=27$) generates more backscattered electrons than the surrounding Al_2O_3 ($z=15$).

IV. CONCLUSIONS

We have presented a new method for preparing SnO_2 thin films by ALD using alternating exposures to tetrakis(dimethylamino) tin (TDMASn) and H_2O_2 which avoids the problems of corrosion and agglomeration associated with the traditional $SnCl_4$ precursor. SnO_2 films could be deposited at temperatures of 50–300 °C with an average growth rate of 1.2 Å/cycle. *In situ* QCM and QMS measurements revealed that approximately three of every four dimethylamine ligands are released during the TDMASn adsorption step. SEM images show that the SnO_2 films are smooth, conformal, and nearly featureless in accord with the finding that the SnO_2 films are amorphous by XRD. AFM measured a surface roughness of only 0.84 nm for a film with a thickness of 92 nm. SnO_2 films with a thickness of 140 nm deposited at 150 °C are fairly conductive ($\rho=0.3$ Ω cm) and highly transparent ($T=94\%$). This method allows, for the first time, low temperature (50 °C) growth of SnO_2 films by ALD. However, XPS measurements reveal that some residual dimethylamine ligands remain in the films deposited below 150 °C. Finally, we show that this process is suitable for conformally coating high aspect ratio anodic alumina membranes relevant to solar cell fabrication.

ACKNOWLEDGMENTS

The work at Argonne is supported by the U.S. Department of Energy, BES-Materials Sciences under Contract No. W-31-109-ENG-38. The work at Northwestern University is supported by the U.S. Department of Energy, Basic Energy Sciences Program under Grant No. DE-FG02-87ER13808.

[1] C. Beneking, B. Rech, S. Wieder, O. Kluth, H. Wagner, W. Frammelsberger, R. Geyer, P. Lechner, H. Rubel, and H. Schade, Thin Solid Films **351**, 241 (1999).
[2] X. J. Huang, Y. K. Choi, K. S. Yun, and E. Yoon, Sens. Actuators B **115**, 357 (2006).
[3] H. M. Yang, X. C. Zhang, and A. D. Tang, Nanotechnology **17**, 2860 (2006).
[4] V. Simakov, O. Yakusheva, A. Grebennikov, and V. Kisin, Sens. Actuators B **116**, 221 (2006).
[5] C. J. Jin, T. Yamazaki, K. Ito, T. Kikuta, and N. Nakatani, Vacuum **80**, 723 (2006).
[6] A. Rosental, A. Tarre, A. Gerst, T. Uustare, and V. Sammelselg, Sens. Actuators B **77**, 297 (2001).
[7] A. Hagemeyer, Z. Hogan, M. Schlichter, B. Smaka, G. Streukens, H. Turner, A. Volpe, H. Weinberg, and K. Yaccato, Appl. Catal., A **317**, 139 (2007).
[8] H. Hosono, H. Ohta, M. Orita, K. Ueda, and M. Hirano, Vacuum **66**, 419 (2002).
[9] G. F. Wang, X. M. Tao, and H. M. Huang, Color. Technol. **121**, 132 (2005).
[10] M. Vergohl, N. Malkomes, T. Matthee, G. Brauer, U. Richter, F. W. Nickol, and J. Bruch, Thin Solid Films **392**, 258 (2001).
[11] M. Adnane, H. Cachet, G. Folcher, and S. Hamzaoui, Thin Solid Films **492**, 240 (2005).
[12] H. Viirola and L. Niinisto, Thin Solid Films **251**, 127 (1994).
[13] V. Shrotriya, G. Li, Y. Yao, C. W. Chu, and Y. Yang, Appl. Phys. Lett. **88**, 073508 (2006).
[14] U. Betz, M. K. Olsson, J. Marthy, M. F. Escolá, and F. Atamny, Surf. Coat. Technol. **200**, 5751 (2006).
[15] Y. Liu, W. Zhu, O. K. Tan, X. Yao, and Y. Shen, J. Mater. Sci.: Mater. Electron. **7**, 279 (1996).
[16] H. Viirola and L. Niinisto, Thin Solid Films **249**, 144 (1994).
[17] X. Du, Y. Du, and S. M. George, J. Vac. Sci. Technol. A **23**, 581 (2005).

[18]J. Sundqvist, J. Lu, M. Ottosson, and A. Harsta, Thin Solid Films **514**, 63 (2006).
[19]M. Ritala and M. Leskela, in *Handbook of Thin Film Materials*, edited by H. S. Nalwa (Academic, San Diego, 2001), Vol. 1, p. 103.
[20]M. J. Pellin, P. C. Stair, G. Xiong, J. W. Elam, J. Birrell, L. Curtiss, S. M. George, C. Y. Han, L. Iton, H. Kung, M. Kung, and H. H. Wang, Catal. Lett. **102**, 127 (2005).
[21]J. W. Elam, D. Routkevitch, P. P. Mardilovich, and S. M. George, Chem. Mater. **15**, 3507 (2003).
[22]T. Asikainen, M. Ritala, and M. Leskela, J. Electrochem. Soc. **141**, 3210 (1994).
[23]R. L. Puurunen, Chem. Vap. Deposition **11**, 79 (2005).
[24]G. Choi, L. Satyanarayana, and J. Park, Appl. Surf. Sci. **252**, 7878 (2006).
[25]W. Lee, K. Hong, Y. Park, N. H. Kim, Y. Choi, and J. Park, Electron. Lett. **41**, 475 (2005).
[26]W. Lee, Y. Choi, K. Hong, N. H. Kim, Y. Park, and J. Park, J. Korean Phys. Soc. **46**, L756 (2005).
[27]A. B. F. Martinson, J. W. Elam, J. T. Hupp, and M. J. Pellin, Nano Lett. **7**, 2183 (2007).
[28]J. W. Elam, A. B. F. Martinson, M. J. Pellin, and J. T. Hupp, Chem. Mater. **18**, 3571 (2006).
[29]G. T. Lim and D. H. Kim, Thin Solid Films **498**, 254 (2006).
[30]R. Katamreddy, R. Inman, G. Jursich, A. Soulet, A. Nicholls, and C. Takoudis, Thin Solid Films **515**, 6931 (2007).
[31]C. L. Dezelah, O. M. El-Kadri, I. M. Szilagyi, J. M. Campbell, K. Arstila, L. Niinisto, and C. H. Winter, J. Am. Chem. Soc. **128**, 9638 (2006).
[32]D. M. Hausmann, E. Kim, J. Becker, and R. G. Gordon, Chem. Mater. **14**, 4350 (2002).
[33]J. W. Elam, M. D. Groner, and S. M. George, Rev. Sci. Instrum. **73**, 2981 (2002).
[34]J. W. Elam and M. J. Pellin, Anal. Chem. **77**, 3531 (2005).
[35]R. L. Puurunen, J. Appl. Phys. **97**, 121301-1 (2005).
[36]Eight Peak Index of Mass Spectra, Mass Spectometry Data Centre, The Royal Society of Chemistry, Cambridge, UK, 1991.
[37]W. J. Maeng and H. Kim, Electrochem. Solid-State Lett. **9**, G191 (2006).
[38]X. Y. Liu, S. Ramanathan, A. Longdergan, A. Srivastava, E. Lee, T. E. Seidel, J. T. Barton, D. Pang, and R. G. Gordon, J. Electrochem. Soc. **152**, G213 (2005).
[39]L. A. Okada and S. M. George, Appl. Surf. Sci. **137**, 113 (1999).
[40]M. Ritala, T. Asikainen, and H. Leskela, Electrochem. Solid-State Lett. **1**, 156 (1998).
[41]A. W. Ott, J. W. Klaus, J. M. Johnson, and S. M. George, Thin Solid Films **292**, 135 (1997).
[42]*The Oxide Handbook*, edited by G. V. Samsonov (IFI/Plenum, New York, 1973), Vol. 1, p. 218.
[43]R. Sanjines, C. Coluzza, D. Rosenfeld, F. Gozzo, P. Almeras, F. Levy, and G. Margaritondo, J. Appl. Phys. **73**, 3997 (1993).
[44]J. Isidorsson, C. G. Granqvist, K. von Rottkay, and M. Rubin, Appl. Opt. **37**, 7334 (1998).
[45]M. Utriainen, H. Lattu, H. Viirola, L. Niinisto, R. Resch, and G. Friedbacher, Mikrochim. Acta **133**, 119 (2000).